New Constraints on the Volatile Deposit in Mercury's North Polar Crater, Prokofiev. Michael K. Barker[1], N. L. Chabot[2], E. Mazarico[1], M. Siegler[3], J. M. Martinez Camacho[3], C. Hamill[4], S. Bertone[5], [1]NASA Goddard Space Flight Center, Greenbelt, MD 20771, USA, [2]Johns Hopkins Applied Physics Laboratory, [3]University of Arizona, [4] Purdue University, [5]University of Maryland Baltimore County.

Introduction: There is strong evidence from multi-wavelength, multi-instrument observations and thermal models for the presence of ice and other volatiles in Mercury's north polar permanently shadowed regions (PSRs) [1-6]. Ground-based radar measurements identified bright regions in some polar craters interpreted to be water ice on or near the surface [1]. The MESSENGER spacecraft found that some radar-bright deposits appeared bright in the optical and near-infrared while others appeared dark [4-6]. The bright regions were interpreted to be exposed surface ice while the dark regions were hypothesized to be complex organic volatile lag deposits overlaying buried ice [3]. One example of the former is in the 112 km diameter crater, Prokofiev, for which the Mercury Dual Imaging System (MDIS) acquired broadband images while in Sun shadow but illuminated by scattered light from the crater walls [5]. These images revealed a relatively high-albedo region spatially correlated with the PSR. Subsequent work [7] found a small offset between the boundary of the radar-bright region and that of the PSR predicted by an illumination model based on the polar digital elevation model (DEM) from the Mercury Laser Altimeter (MLA). Such an offset, if true, could have implications for the ice properties and its delivery and destruction mechanisms. However, the low resolution (1 km/pix) of the polar MLA DEM precluded a definitive conclusion. In the present work, we build new higher-resolution topographic, illumination, and thermal models of Prokofiev to place stronger constraints on its PSR and volatile deposits. We also study the MLA reflectance data in this crater to quantitatively estimate the ice abundance.

New Topographic, Illumination and Thermal Models for Prokofiev: We follow the same procedure we used for 8 other craters hosting subsurface ice and dark surface lag deposits [8]. We apply the Ames Stereo Pipeline (ASP) shape-from-shading (SfS) tool [9] to a set of MDIS images of Prokofiev using a cleaned MLA-only DEM as the *a priori* model. The resulting hybrid MLA+SfS DEM (Fig. 1a), with a pixel scale of 125 m/pix, is more realistic than either an image- or MLA-based DEM alone. MLA topography inside the PSR is included, which is not possible with image-based models, and the crater rim is more realistic, which can be a challenge for MLA-only DEMs. An accurate reconstruction of the rim is important for determining the true extent of the PSR.

The new topographic model allows a more detailed look at the illumination and thermal conditions inside Prokofiev than was possible with the original polar MLA DEM. The PSRs within Prokofiev are visible as dark blue regions in the map of average illumination (Fig. 1b) and are dominated by a large region along the southern portion of the crater and the central peak/crater, with many smaller PSRs inside craters throughout the floor. The large southern PSR also stands out in the thermal model with maximum temperature < 110 K (Fig. 1c) and surface-stable ice (i.e., ice stability depth of 0 m; Fig. 1d). The central crater and most of the smaller floor craters are too warm for stable surface ice. Note, however, that stable surface ice may exist in cold traps unresolved by the DEM [10]. A simulated image including scattered light within the crater (Fig. 2a) reproduces many of the albedo variations in the corresponding MDIS broadband image except for the high-albedo region (Fig. 2b). This confirms earlier lower-resolution scattered light simulations that could not reproduce the high-albedo region [5], and strongly supports that it is a real feature on the surface rather than a result of the topography and the diffuse lighting conditions.

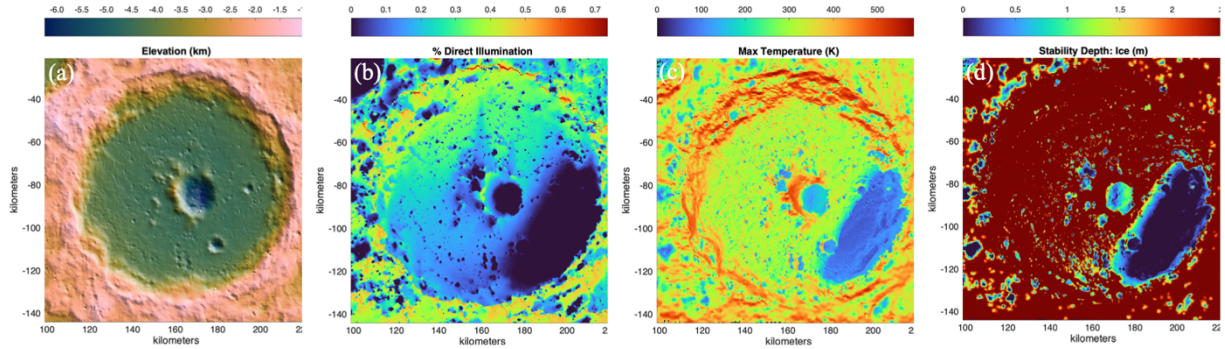

Figure 1 – High-resolution models of Prokofiev. (a) Colorized hillshade of MLA+SfS DEM. (b) Average direct illumination over one Mercury solar day. (c) Maximum surface temperature throughout a Mercury solar day. (d) Depth below the surface needed for the long-term stability of ice. The dark-blue region represents where ice is thermally stable at the surface.

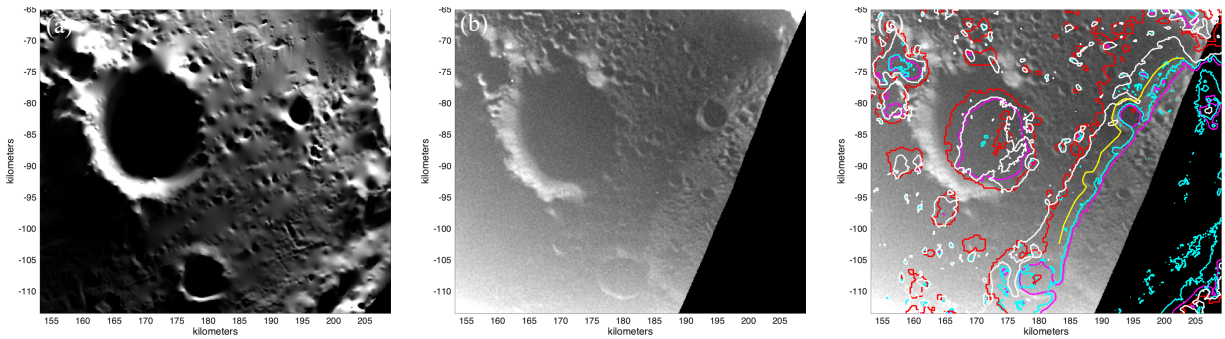

Figure 2 – Comparison between simulations and MDIS broadband image EW1020581108B. (a) Simulated image using the MLA+SfS DEM. (b) MDIS image, (c) MDIS image with contours: PSR (magenta), ice stability depth of 0 m (cyan), MDIS high-albedo boundary (yellow), ice stability depth of 1 m (white), and radar brightness > 4σ (red; based on Fig. 3b of [14]).

Due to their higher resolution and fidelity, the new models allow us to examine the PSR and MDIS high-albedo boundaries with more confidence than previously possible. Fig. 2c compares the PSR, MDIS high-albedo area, surface ice stability zone, and radar-bright region. The radar-bright boundary extends farther than the PSR. This strongly favors the interpretation that this boundary offset is real and not an artifact of inaccuracies in the MLA-only or MLA+SfS DEMs, and makes this region unique on Mercury for being a substantial radar-bright region located outside a PSR.

Mixing Models: To constrain the ice abundance, we use the MLA reflectance (1064 nm normal albedo) dataset since it is free from the confounding effects of viewing and illumination geometry and scattered light [11,12]. Nevertheless, the MLA reflectance was a noisy measurement with systematic instrumental errors that varied throughout the mission as the instrument aged and operating conditions changed, thus requiring careful selection of the most reliable subset of data.

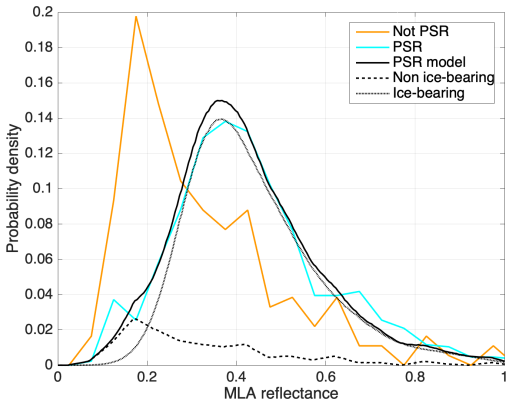

Figure 3 – (a) Distribution of MLA reflectance values inside (cyan) and outside (orange) PSRs on Prokofiev's floor compared to the best-fit linear mixture model (solid black line) assuming $r_i = 0.8$. In this model, 15% of MLA footprints have no ice (long-dashed black line) while 85% have ice (dotted black line) with a 25% sub-footprint areal ice coverage.

We fit the histogram of MLA reflectance values inside the PSR (861 points, cyan line in Fig. 3) as a linear mixture of two end-members: dry regolith with the reflectance distribution given by the 182 points outside the PSR on the crater floor (orange line in Fig. 3) and pure ice with a Gaussian reflectance distribution with mean r_i and standard deviation σ_i. The model has an ice-bearing fraction F_i of MLA footprints (each ~30 – 40 m in diameter), each with a sub-footprint areal ice fraction f_i, and the remaining fraction (1-F_i) of footprints have only dry regolith. A wide range of f_i and r_i produce acceptable fits as these two parameters are highly correlated. Thus, we fix r_i at 0.8, the preferred value from a similar analysis of Lunar Orbiter Laser Altimeter (LOLA) reflectance data at the Moon's south polar PSRs [13]. The resulting best-fit model (solid black line in Fig. 3) has $F_i = 0.85$, $f_i = 0.25$ and $\sigma_i = 0.25$. The ice-bearing footprint fraction, F_i, could lie in the range ~0.7–1.0 while the sub-footprint areal ice fraction f_i could be ~0.15–0.30 and still produce acceptable fits. This suggests that surface ice in Prokofiev has a ~2–4 times higher areal abundance than it does at the Moon's South Pole, where $F_i = 0.25$ and $f_i = 0.07$ [13], but that the surface ice in Prokofiev is also not pure. These new results about the nature of the surface ice in Prokofiev can help constrain the age and origin of Mercury's polar volatile deposits.

References: [1] Harmon, J. K. (2007), *SSR*, 132, 307-349. [2] Lawrence, D. J., et al. (2013) *Science*, 339, 292-296. [3] Paige, D. A., et al. (2013) *Science*, 339, 300-303. [4] Neumann, G. A., et al. (2013) *Science*, 339, 296-300. [5] Chabot, N. L., et al. (2014), *Geology*, 42, 1051-1054. [6] Chabot, N. L., et al. (2016), *GRL*, 43, 9461-9468. [7] Deutsch, A. N, et al. (2016), *Icarus*, 280, 158-171. [8] Hamill, C., et al. (2020) *PSJ*, 1, 57. [9] Alexandrov, O. & Beyer, R. A. (2018) *ESS*, 5, 652-666. [10] Rubanenko, L., et al. (2018) *JGR: Planets*, 123, 2178-2191. [11] https://pgda.gsfc.nasa.gov/products/64 [12] Deutsch, A. N., et al. (2017) *GRL*, 44, 9233-9241. [13] Fisher, E. A., et al. (2017), *Icarus*, 292, 74-85. [14] Harmon, J. K., et al. (2011), *Icarus*, 211, 37-50.